A&A 630, A88 (2019)
https://doi.org/10.1051/0004-6361/201935138


Astronomy & Astrophysics

# J-PLUS: Impact of bars on quenching timescales in nearby green valley disc galaxies

J. P. Nogueira-Cavalcante[1], R. Dupke[1,2], P. Coelho[3], M. L. L. Dantas[3,4], T. S. Gonçalves[5], K. Menéndez-Delmestre[5], R. Lopes de Oliveira[1,6,16], Y. Jiménez-Teja[1], C. López-Sanjuan[12], J. Alcaniz[1], R. E. Angulo[15], A. J. Cenarro[12], D. Cristóbal-Hornillos[12], C. Hernández-Monteagudo[12], A. Ederoclite[3], A. Marín-Franch[12], C. Mendes de Oliveira[3], M. Moles[12], L. Sodré Jr.[3], J. Varela[12], H. Vázquez Ramió[12], A. Alvarez-Candal[1], A. Chies-Santos[8], L. A. Díaz-García[12], L. Galbany[14], J. Hernandez-Jimenez[3,9], P. Sánchez-Blázquez[11], M. Sánchez-Portal[13], D. Sobral[7], E. Telles[1], and E. Tempel[10]

*(Affiliations can be found after the references)*

Received 26 January 2019 / Accepted 11 July 2019

**ABSTRACT**

*Context.* Between the blue cloud and the red sequence peaks on the galaxy colour–magnitude diagram there is a region sparsely populated by galaxies called the green valley. In a framework where galaxies mostly migrate on the colour–magnitude diagram from star forming to quiescent, the green valley is considered a transitional galaxy stage. The details of the processes that drive galaxies from star-forming to passive systems still remain unknown.

*Aims.* We aim to measure the transitional timescales of nearby galaxies across the green valley, through the analysis of Galaxy Evolution Explorer and Javalambre Photometric of Local Universe Survey photometric data. Specifically, we seek to study the impact of bars on the quenching timescales.

*Methods.* We developed a method that estimates empirically the star formation quenching timescales of green valley galaxies, assuming an exponential decay model of the star formation histories and through a combination of narrow and broad bands from the Javalambre Photometric of Local Universe Survey and Galaxy Evolution Explorer. We correlated these quenching timescales with the presence of bars.

*Results.* We find that the Javalambre Photometric of Local Universe Survey colours F0395 $-g$ and F0410 $-g$ are sensitive to different star formation histories, showing, consequently, a clear correlation with the $D_n(4000)$ and $H_{\delta A}$ spectral indices. We measured quenching timescales based on these colours and we find that quenching timescales obtained with our new approach are in agreement with those determined using spectral indices. We also compared the quenching timescales of green valley disc galaxies as a function of the probability of hosting a bar. We find that galaxies with high bar probability tend to quench their star formation slowly.

*Conclusions.* We conclude that: (1) Javalambre Photometric of Local Universe Survey filters can be used to measure quenching timescales in nearby green valley galaxies; and (2) the resulting star formation quenching timescales are longer for barred green valley galaxies. Considering that the presence of a bar indicates that more violent processes (e.g. major mergers) are absent in host galaxies, we conclude that the presence of a bar can be used as a morphological signature for slow star formation quenching.

**Key words.** galaxies: evolution – galaxies: spiral – galaxies: star formation – galaxies: stellar content – galaxies: structure

## 1. Introduction

It is now well known that galaxies in the local Universe can generally be separated into two broad classifications with respect to their star formation activity: blue star-forming (blue cloud) galaxies, composed mostly of disc galaxies, and red passive systems (red sequence) typically composed of elliptical and lenticular galaxies with little or no recent star formation (e.g. Strateva et al. 2001; Kauffmann et al. 2003; Shen et al. 2003; Baldry et al. 2004; Balogh et al. 2004; Menci et al. 2005). The star formation rate (SFR) of blue galaxies is well correlated with their stellar mass ($M_*$), defining the main sequence of star-forming galaxies in the SFR–$M_*$ plane (Brinchmann et al. 2004; Salim et al. 2007; Gilbank et al. 2010; McGee et al. 2011). This correlation was already in place at $z \sim 1$ (Willmer et al. 2006; Noeske et al. 2007) and possibly at $z \geq 2$ (e.g. Brammer et al. 2009; Taylor et al. 2009; Whitaker et al. 2012; Speagle et al. 2014). Most tellingly, the number density of red passive galaxies has roughly doubled since $z \sim 1$, while the number of blue galaxies has remained nearly constant (Bell et al. 2004; Brown et al. 2007; Faber et al. 2007; Ilbert et al. 2013; Muzzin et al. 2013; Sobral et al. 2014). This motivates the search for processes that cause blue, star-forming galaxies to transition to red, non-star-forming ones. This transition has become known as quenching.

Between the blue cloud and the red sequence peaks on galaxy colour–magnitude diagrams (CMD), there is a narrow region, sparsely populated by galaxies, known as the green valley (Martin et al. 2007; Salim et al. 2007; Wyder et al. 2007; Schawinski et al. 2014; Renzini & Peng 2015; Smethurst et al. 2015; Díaz-García et al. 2018; Nogueira-Cavalcante et al. 2018). The physical properties of galaxies in the green valley region are different from those in either the blue cloud or the red sequence, exhibiting intermediate characteristics, for instance the age of stellar population and local environment (Pan et al. 2013), the specific star formation rate (Salim 2014), and galaxy structures parametrized by Sérsic indices (Bremer et al. 2018). The intermediate nature of the green valley suggests that green valley galaxies are quenching their star formation, starting in the blue cloud phase and reaching the red sequence afterwards. The typical quenching timescales, that is, the duration of the green

valley phase, is a function of cosmic time; the galaxy transition across the green valley in the local Universe ($z < 0.2$) takes, on average, ∼1−2 Gyr (Martin et al. 2007; Bremer et al. 2018), whereas at intermediate redshifts ($z \sim 0.7$) the average green valley quenching phase lasts less than 500 Myr (Gonçalves et al. 2012). External events can trigger new episodes of star formation in quiescent red galaxies, becoming bluer through the CMD. Pan et al. (2014) found that more than 50% of green valley early-type galaxies at $0.02 < z < 0.05$ have blue central cores, supporting a scenario of recent gas-rich mergers. This result is in agreement with simulations that predict that up to ∼17% of green valley galaxies at $z < 2$ are passive galaxies which are increasing their star formation activity (Trayford et al. 2016). These galaxies could be early-type galaxies that live in the centres of galaxy clusters and occasionally capture a lower mass gas-rich galaxy (e.g. Martin et al. 2017; Darvish et al. 2018). However, it is observed that the red sequence region has grown, at least since $z \sim 1$ (Bell et al. 2004; Brown et al. 2007; Faber et al. 2007; Ilbert et al. 2013; Muzzin et al. 2013) and, therefore, it is reasonable to consider that, for the majority of galaxies, the galaxy transition on the CMD is from the blue cloud to the red sequence, passing through the green valley.

Many possible quenching mechanisms that lead galaxies to the green valley have been proposed for both low and high redshifts. Overall, these mechanisms can be classified as rapid processes, meaning those able to quench star formation on a scale of hundreds of millions of years, and slow processes, which take more than 1 Gyr to completely quench star formation. Rapid processes can encompass, for instance, negative feedback from active galactic nuclei (AGN; e.g. Di Matteo et al. 2005; Springel et al. 2005a; Ciotti & Ostriker 2007; Cattaneo et al. 2009; Martin et al. 2007; Schawinski et al. 2009; Dubois et al. 2013; Bongiorno et al. 2016; Smethurst et al. 2016; Kocevski et al. 2017), major mergers (e.g. Toomre 1977; Springel et al. 2005b; Conselice 2006), and violent disc instability (e.g. Dekel & Burkert 2014; Zolotov et al. 2015; Nogueira-Cavalcante et al. 2019). These mechanisms are claimed to explain the formation of most passive dead galaxies. Stellar feedback (e.g. Menci et al. 2005; Lagos et al. 2013) is another example of a rapid process and is generally claimed to explain quenching in low-mass galaxies. Slow processes can involve interactions in clusters and groups (e.g. Gunn & Gott 1972; White 1976; Hausman & Ostriker 1978; Moore et al. 1998; Abadi et al. 1999; Balogh et al. 1999, 2004; Boselli et al. 2006; Capak et al. 2007; Moran et al. 2007; van den Bosch et al. 2008; Wetzel et al. 2013; Peng et al. 2015; Darvish et al. 2016, 2018; Hatfield & Jarvis 2017; Smethurst et al. 2017; van de Voort et al. 2017) and secular evolution through internal galaxy structures like spiral arms and, especially, stellar bars (e.g. Kormendy & Kennicutt 2004; Sheth et al. 2005; Masters et al. 2010, 2011; Mendez et al. 2011; Cheung et al. 2013). Although different galaxy mechanisms can act simultaneously, observations suggest that quenching processes that correlate with stellar mass are independent from those that correlate with galaxy environment (Peng et al. 2010; Sobral et al. 2014).

Even though the details concerning the physical processes responsible for the galaxy transition across the green valley are not known, recent works have given clues on how quenching processes act in galaxies. Rowlands et al. (2018) found that, at $z < 1$, the red sequence grows faster for intermediate-mass galaxies ($M_\star > 10^{10.6}\,M_\odot$) than for those with high stellar masses ($M_\star > 10^{11}\,M_\odot$). Furthermore, evidence for multiple evolutionary quenching pathways has been shown by Schawinski et al. (2014) and Maltby et al. (2018) for galaxies at low and high redshifts, respectively. These results suggest that multiple quenching processes act simultaneously and in different ways at different cosmic times. Therefore, the green valley must present different characteristics in different epochs of the Universe, since, by definition, it is a transitional region of galaxies. In fact, the population of green valley galaxies is different in the local Universe, exhibiting mostly S0 and Sa disc morphologies (Salim 2014; Schawinski et al. 2014; Evans et al. 2018; Bremer et al. 2018), as opposed to those at intermediate redshifts, which often exhibit elliptical and distorted morphologies (Nogueira-Cavalcante et al. 2018). These general results suggest that violent processes (associated with more elliptical and distorted morphologies at intermediate redshifts) are more frequent for a younger Universe whereas secular evolution is more common at low redshifts.

A useful way to understand how galaxies transition from the blue cloud to the red sequence is by measuring how long it takes for galaxies to cross the green valley. Martin et al. (2007) developed a method that estimates quenching timescales for green valley galaxies (Sect. 2), based on photometry and spectroscopy from the Sloan Digital Sky Survey (SDSS; York et al. 2000) and photometry from the Galaxy Evolution Explorer (GALEX; Martin et al. 2005). However, one difficulty with this method is the need for spectroscopic data. Big spectroscopic surveys, like SDSS, zCOSMOS (Lilly et al. 2007), and Large Early Galaxy Astrophysics Census (LEGA-C; van der Wel et al. 2016; Straatman et al. 2018) pre-select only the brightest galaxies. Moreover, in the case of SDSS galaxy spectra, the fiber diameter is 3″, restricting observations to the centre of nearby galaxies.

In this work, we develop a new approach to estimate quenching timescales in green valley galaxies, which circumvents this difficulty; it is based on the Martin et al. (2007) method but uses only photometric galaxy data. The lack of spectra is compensated for by the narrow band filters of the photometric system of the Javalambre Photometric of Local Universe Survey[1] (J-PLUS, Cenarro et al. 2019). This is an ancillary survey of the Javalambre Physics of the accelerating universe Astrophysical Survey[2] (J-PAS, Benitez et al. 2014), which will observe 8500 deg$^2$ of the sky with 56 narrow band filters. J-PLUS observations are carried out from the Javalambre Observatory in Spain, with the Javalambre Auxiliary Survey Telescope (JAST/T80), which is a 0.83 m telescope, equipped with the T80Cam camera, supplying a field of view of 3 deg$^2$ at a pixel-scale of 0.55″. Additionally, its filter set is composed of a total of 12 optical filters: four broad ($g$, $r$, $i$, and $z$), two intermediate ($u$JAVA and F0861), and six narrow (F0378, F0395, F0410, F0430, F0515, and F0660).

In this work we show the application of this new approach in a sample of nearby green valley disc galaxies and we analyse the dependence of the measured quenching timescales of these galaxies on their probability of hosting a bar. Stellar bars are present in more than half of nearby spiral galaxies (e.g. Menéndez-Delmestre et al. 2007; Sheth et al. 2008; Masters et al. 2011) and are associated with the redistribution of angular momentum of the baryonic and dark matter components (Sellwood 1981; Athanassoula 2003; Athanassoula et al. 2013; Machado & Athanassoula 2010), formation of rings and lens structures (Kormendy & Kennicutt 2004), induction of star formation activity in the central parts of host galaxies (Sheth et al. 2005; Coelho & Gadotti 2011; Oh et al. 2012; Wang et al. 2012), formation of pseudobulges (Sheth et al. 2005;

[1] www.j-plus.es
[2] www.j-pas.org

Méndez-Abreu et al. 2008; Aguerri et al. 2009), and possibly feeding active galactic nucleus (AGN) activity (Shlosman et al. 1989; Ho et al. 1997; Oh et al. 2012).

We structure this paper as follows. In Sect. 2 we describe the original method by Martin et al. (2007) to measure quenching timescales and our new approach based on that method. In Sect. 3 we apply our method to nearby green valley disc galaxies and analyse how their morphological parameters can impact quenching timescales. In Sect. 4 we discuss the robustness of our approach. The results are summarized in Sect. 5. Throughout this paper we adopt AB magnitudes and standard ΛCDM cosmology: $H_0 = 70\,\mathrm{km\,s^{-1}\,Mpc^{-1}}$, $\Omega_\mathrm{m} = 0.30$, and $\Omega_\Lambda = 0.70$.

## 2. Measuring star formation quenching timescales in green valley galaxies

In this work we develop a method that estimates quenching timescales in nearby green valley galaxies, using J-PLUS and GALEX photometric data and based on the work described in Martin et al. (2007). The main difficulty with this approach with J-PLUS data is that we cannot directly compare the J-PLUS magnitudes with SDSS spectral indices due to the limited fiber aperture of 3″ in the diameter of SDSS spectra. For instance, up to $z \sim 0.2$ only the bulge of a Milky-Way-like galaxy is observed with such an aperture. One way to circumvent this issue is through constructing J-PLUS spectral energy distributions (SED) from SDSS spectra. To that end, we used a `python` package called `pysynphot` (Lim et al. 2015; STScI development Team 2013) as well as the appropriate parameters given the configuration of the survey properties (for further details we refer the reader to Cenarro et al. 2019). In the next sections we describe the selection of green valley galaxies in SDSS data, the original Martin et al. (2007) method that this work is based on, and our new approach that measures quenching timescales in green valley galaxies from J-PLUS photometry.

### 2.1. Selection of green valley galaxies

We selected green valley galaxies from the traditional galaxy CMD (Fig. 1) using two broad bands: the near-ultraviolet (NUV) band from GALEX GR6/GR7 (Martin et al. 2005), and the $r$ band from SDSS DR12 (Alam et al. 2015). We retrieved spectra and photometry from the GALEX CasJobs database[3] and following the selection criteria of Martin et al. (2007): redshift range of $0.0 < z < 0.2$; NUV weight $> 800$; NUV artefact $< 2$; apparent NUV magnitude $< 23$; and apparent $r$ magnitude $< 17.7$. We cross-matched SDSS and GALEX samples within a radius of 1″ and applied the Seaton (1979) model to correct for Galactic extinction. In addtion we applied $k$-correction in SDSS and GALEX magnitudes using the $k$-correction calculator (the `python` version of the $k$-correction calculator[4], Chilingarian et al. 2010; Chilingarian & Zolotukhin 2012). We used the definition of the green valley on the CMD as the region between $4.0 < \mathrm{NUV} - r < 5.0$, as estimated by previous works (e.g. Martin et al. 2007; Gonçalves et al. 2012; Salim 2014; Nogueira-Cavalcante et al. 2018, 2019). From the green valley sample, we sub-selected those galaxies with an error of $\mathrm{H}_{\delta,A}$ spectral index lower than 1 Å. This is a necessary condition to properly determine the best star formation history model from stellar population synthesis codes (see Sect. 2.2 and also Gonçalves et al. 2012). With these constraints, the initial number of green valley galaxies is comprised of 2865 objects.

The green valley is not only populated by transitional galaxies but also by star-forming galaxies obscured by dust. We properly correct galaxy magnitudes through the flux of the $\mathrm{H}_\alpha$ and $\mathrm{H}_\beta$ emission lines, estimating the excess in $B - V$ colour, $E(B-V)$, following the prescription by Calzetti et al. (1994),

$$E(B-V) = 0.935 \ln\left(\frac{\mathrm{H}_\alpha/\mathrm{H}_\beta}{2.88}\right) \times 0.44, \quad (1)$$

where the term 0.44 takes into account that we are estimating stellar continuum extinction through nebular emission (Calzetti et al. 1994). In other words, the extinction in the stellar continuum is roughly half of the value for ionized gas. To convert $E(B-V)$ into extinction in SDSS and GALEX magnitudes we use the relation

$$A_\lambda = k_\lambda \times E(B-V), \quad (2)$$

where $A_\lambda$ is the extinction in magnitudes at the wavelength $\lambda$ and $k_\lambda$ is the extinction curve by Calzetti et al. (2000). For $0.12 \leq \lambda\,[\mu\mathrm{m}] \leq 0.63$,

$$k(\lambda) = 1.17\left(-2.156 + \frac{1.509}{\lambda} - \frac{0.198}{\lambda^2} + \frac{0.011}{\lambda^3}\right) + 1.78, \quad (3)$$

and for $0.63 \leq \lambda\,[\mu\mathrm{m}] \leq 2.20$,

$$k(\lambda) = 1.17\left(-1.857 + \frac{1.040}{\lambda}\right) + 1.78. \quad (4)$$

The CMD corrected by intrinsic dust extinction is shown in Fig. 1. The final number of green valley galaxies is 2043, after excluding star-forming galaxies obscured by dust from the initial sample.

### 2.2. Martin et al. (2007) method

This method considers a very simple parametric model for the star formation histories (SFHs) of green valley galaxies (Fig. 2): a constant star formation rate for the first billions of years, which corresponds to the blue cloud phase, followed by a period of exponential decay (green valley phase):

$$\mathrm{SFR}(t) = \mathrm{SFR}(t_i), \qquad \text{for } t < t_i, \quad (5)$$

$$\mathrm{SFR}(t) = \mathrm{SFR}(t_i)\,\mathrm{e}^{-\gamma(t-t_i)}, \qquad \text{for } t > t_i, \quad (6)$$

where $t_i$ is a characteristic time and the exponential index ($\gamma$) is in units of $\mathrm{Gyr}^{-1}$. This model is not strictly sensitive to $t_i$ (see Fig. 3), since the parameters used to estimate $\gamma$ evolve very weakly during the star-forming phase (for full details see Nogueira-Cavalcante et al. 2018). For instance, Martin et al. (2007) used $t_i = 10$ Gyr, whereas Gonçalves et al. (2012) and Nogueira-Cavalcante et al. (2018, 2019) used $t_i = 6$ Gyr. In this work we consider $t_i = 3$ Gyr, which corresponds to the peak of star formation density of the Universe (e.g. Madau & Dickinson 2014). It is worth mentioning that the only constraint is that $t_i$ must be greater than zero. The $\gamma$ index is the free parameter of this method, which reflects the speed of quenching (for smaller $\gamma$, slower quenching; larger $\gamma$, faster quenching). The inverse of the exponential index ($1/\gamma$) corresponds to a timescale during which the star formation rate decreases by ∼37% from the initial star formation rate before the quenching phase ($e$-folding time). We call this timescale hereafter the quenching timescale.

[3] https://galex.stsci.edu/casjobs/
[4] http://kcor.sai.msu.ru/getthecode/

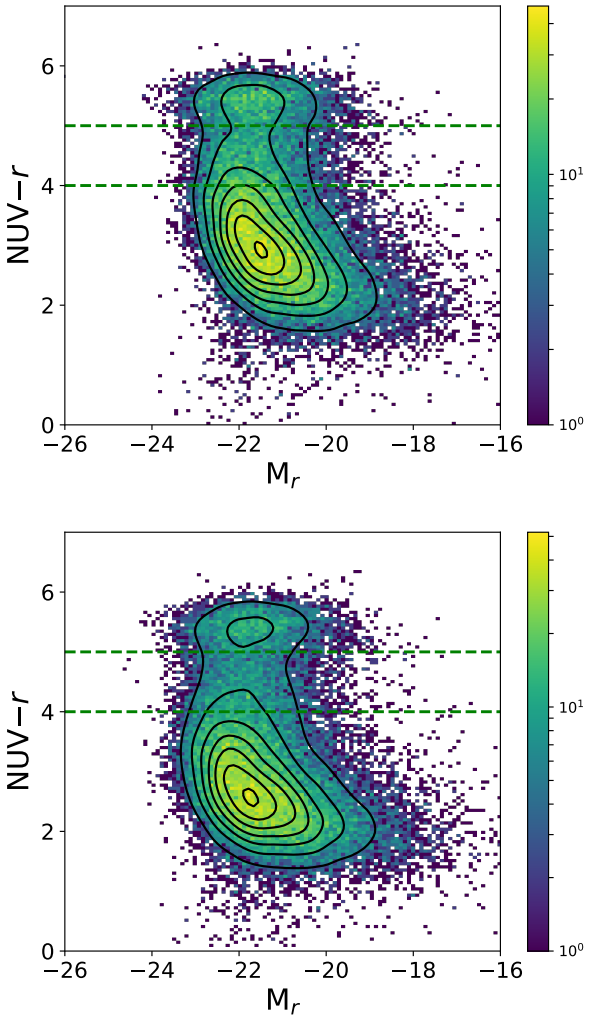


**Fig. 1.** Colour–magnitude diagrams of SDSS+GALEX galaxies at $z < 0.2$, uncorrected (*top panel*) and corrected (*bottom panel*) by intrinsic extinction caused by dust. The horizontal dashed lines represent the green valley region. Each contour line represents approximately the same number of galaxies. The colours in the vertical bar on both panels identify the number of galaxies for each bin within the diagrams.

To estimate $\gamma$ indices for green valley galaxies, Martin et al. (2007) consider three different observables, measured in the rest-frame: one photometric, the NUV $-r$, and two spectroscopic, the 4000 Å break ($D_n(4000)$, Bruzual 1983) and $H_\delta$ absorption line ($H_{\delta,A}$, Worthey & Ottaviani 1997). These indices are defined as

$$D_n(4000) = \sum_{\lambda=4000\,\text{Å}}^{4100\,\text{Å}} F_\lambda \Big/ \sum_{\lambda=3850\,\text{Å}}^{3950\,\text{Å}} F_\lambda \tag{7}$$

and

$$H_{\delta,A} = \sum_{\lambda=4083.5\,\text{Å}}^{4122.25\,\text{Å}} \left(1 - \frac{F_\lambda}{F_{\lambda,\text{cont}}}\right) \mathrm{d}\lambda, \tag{8}$$

where $F_{\lambda,\text{cont}}$ is the continuum flux, defined by a straight line through the average flux density (in Å) between 4041.60–4079.75 and 4128.50–4161.00.

Thus, the $\gamma$ index is a function of these parameters, that is, $\gamma(\text{NUV} - r, D_n(4000), H_{\delta,A})$. Particularly, the $D_n(4000)$ and $H_{\delta,A}$ spectral indices define a well-established plane, where each position indicates a different galaxy star formation history (SFH; Kauffmann et al. 2003). Figure 3 shows a $H_{\delta,A} \times D_n(4000)$ plane, where coloured curves represent the expected temporal evolution of the values of these spectral indices from a stellar population synthesis model, considering the star formation history described by Eqs. (5) and (6). We use five different $\gamma$ values to reproduce these curves: 0.5 $\text{Gyr}^{-1}$, 1 $\text{Gyr}^{-1}$, 2 $\text{Gyr}^{-1}$, 5 $\text{Gyr}^{-1}$ , and 10 $\text{Gyr}^{-1}$, using Bruzual & Charlot (2003) models, with solar metallicities, Padova 1994 stellar evolutionary tracks (Alongi et al. 1993; Bressan et al. 1993; Fagotto et al. 1994a,b), and the initial mass function from Chabrier (2003). The black dots for each colour line on these planes represent the exact predicted value from Bruzual & Charlot (2003) models for a specific NUV $-r$ colour. In other words, for different NUV $-r$ colours there are different values of the spectral indices for the same SFHs. We also show in Fig. 3 the $H_{\delta,A} \times D_n(4000)$ plane for different values of $t_i$ (1 Gyr, 3 Gyr, and 6 Gyr). The position of the black dots does not change considerably for different values of $t_i$, demonstrating that our model is weakly dependent on the $t_i$ parameter.

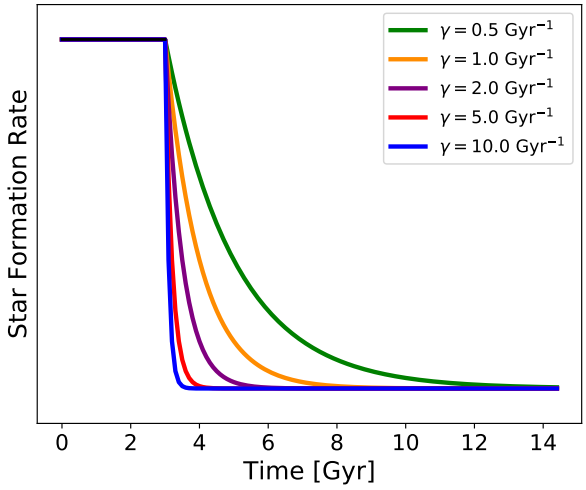


**Fig. 2.** Star formation rate models for five different $\gamma$ values considered in this work (Eqs. (5) and (6)).

However, the SFHs of real green valley galaxies are more complex than those described by Eqs. (5) and (6), reflecting a dispersed distribution of green valley spectral indices on the $H_{\delta,A} \times D_n(4000)$ plane (grey curves in Fig. 3). Therefore, we expect that the spectral indices measured from green valley galaxy spectra are not exactly those predicted from Bruzual & Charlot (2003) models. To take this into account the $H_{\delta,A} \times D_n(4000)$ plane is divided into parts, so that between two consecutive points (dots) we define a perpendicular bisector, which corresponds to the geometric average of the two values. For instance, between the dots that correspond to 0.5 $\text{Gyr}^{-1}$ and 1 $\text{Gyr}^{-1}$ the bisector corresponds to ~0.707 $\text{Gyr}^{-1}$. We interpolate the entire $H_{\delta,A} \times D_n(4000)$ plane, associating each coordinate to a single specific $\gamma$ value (for more details see Nogueira-Cavalcante et al. 2018).

### 2.3. New photometry-only approach with J-PLUS

We seek a set of J-PLUS filters that can efficiently substitute the $D_n(4000)$ and $H_{\delta,A}$ spectral indices. Therefore, for each SDSS spectrum we estimate a J-PLUS SED in the F0395, F0410, and *g* J-PLUS filters. We chose these filters because they lie approximately in the same region of the $D_n(4000)$ and $H_{\delta,A}$ spectral

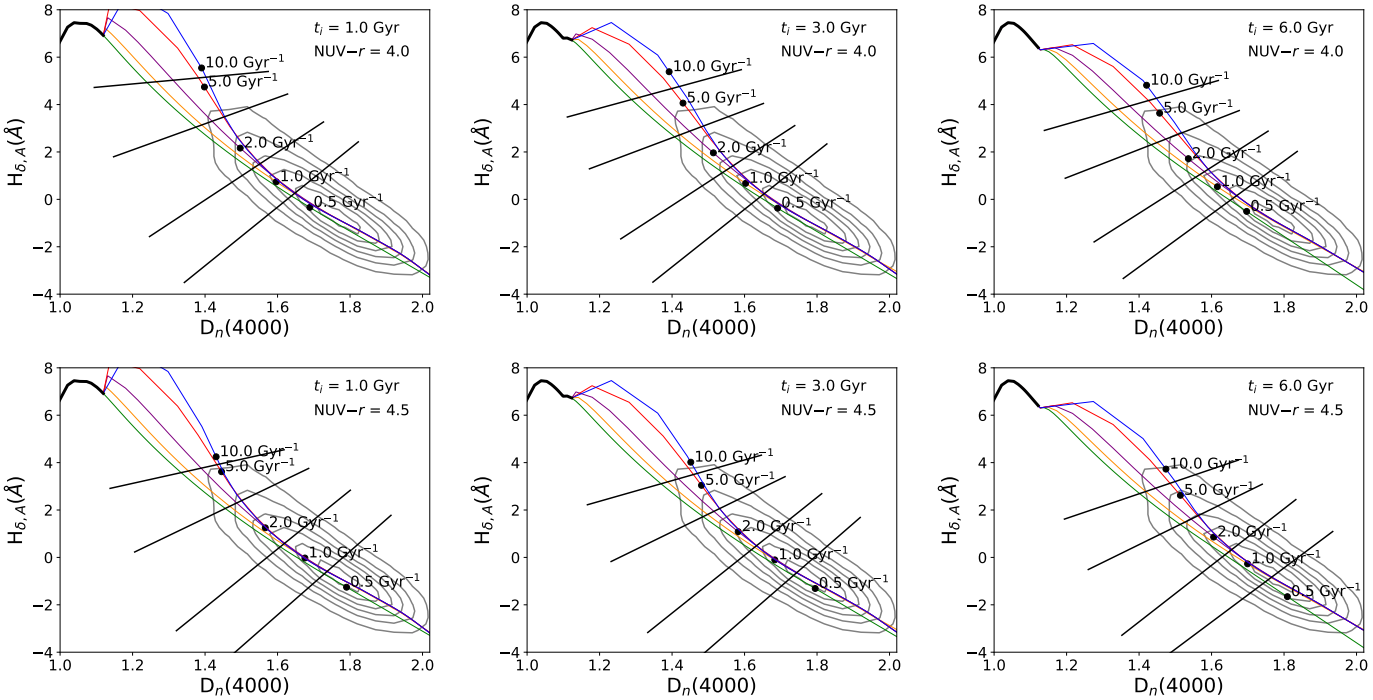


**Fig. 3.** Evolution of $H_{\delta,A} \times D_n(4000)$ planes, considering five $\gamma$ values from the SFH model described in Eqs. (5) and (6) (0.5 Gyr$^{-1}$, 1 Gyr$^{-1}$, 2 Gyr$^{-1}$, 5 Gyr$^{-1}$, and 10 Gyr$^{-1}$). The black dots represent the spectral indices on the planes for a specific SFH and NUV $-r$ colour. Different NUV $-r$ colours show different spectral indices for the same SFH. The grey contours are the distribution of the spectral indices of green valley galaxies measured from SDSS spectra. The straight lines are a geometric average of the spectroscopic indices of two consecutive black dots, dividing the plane into parts and allowing us to computationally interpolate it. For different values of $t_i$ the position of the black dots does not change considerably, demonstrating that our model is weakly dependent on the $t_i$ parameter.

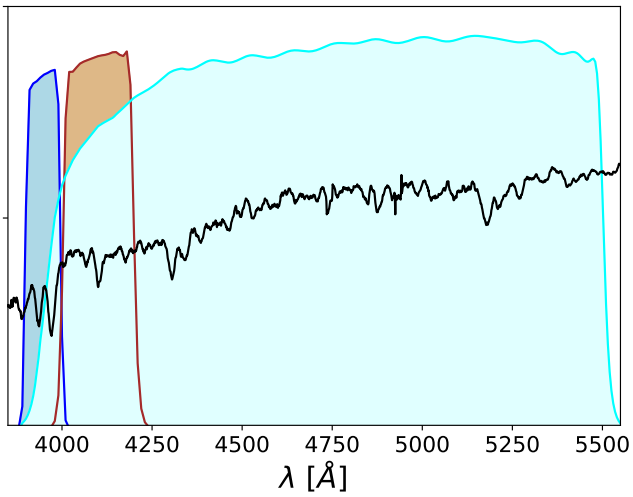


**Fig. 4.** Example of a SDSS green valley galaxy spectrum with three J-PLUS filter responses (F0395 in blue, F0410 in brown, and gSDSS in cyan). The F0395 and F0410 filters straddle the 4000 Å break region, whereas the $H_{\delta,A}$ absorption line (4102 Å) is right in the middle of the F0410 filter.

indices, as shown in Fig. 4. Figures 5 and 6 show the F0395 $-g$ and F0410 $-g$ colours as functions of $D_n(4000)$ and $H_{\delta,A}$ spectral indices, respectively. There are clear correlations amongst these quantities, demonstrating that, in principle, these colours can be used instead of the $D_n(4000)$ and $H_{\delta,A}$ spectral indices to estimate quenching timescales.

Figure 7 shows the same distribution of green valley galaxies and the curves predicted by Bruzual & Charlot (2003) models as in Fig. 3, but now on the F0410 $-$ $g$ $\times$ F0395 $-$ $g$ plane. The procedure to estimate $\gamma$ indices from this diagram is similar to that followed with the $H_{\delta,A} \times D_n(4000)$ plane. For each two consecutive points, which correspond to the predicted values by Bruzual & Charlot (2003) models for a specific NUV $-r$ value, we constructed a bisector, corresponding to the geometric average of the involved dots. Following this procedure we divided all the F0410 $-$ $g$ $\times$ F0395 $-$ $g$ plane into parts, in a similar way to Martin et al. (2007)'s division of the $H_{\delta,A} \times D_n(4000)$ plane. We then compared the estimated quenching timescales between Martin et al. (2007) and our new approach (Fig. 8).

## 3. Star formation quenching timescales in nearby green valley disc galaxies and constraints with bars

By cross-matching the green valley galaxies selected from Fig. 1 with J-PLUS Data Release 1[5] (DR1) and the morphological catalogue from Domínguez Sánchez et al. (2018), we identified which galaxies in our sample were observed by J-PLUS and characterized their probability of hosting a bar. In the following, we describe Domínguez Sánchez et al. (2018)'s catalogue and our results, associating quenching timescales of green valley disc galaxies with the probability of a galaxy hosting a bar (hereafter bar probability).

### 3.1. Morphological catalogue

The Domínguez Sánchez et al. (2018) catalogue classifies morphologically ~670 000 galaxies from SDSS galaxy images. The

[5] www.j-plus.es/datareleases/data_release_dr1

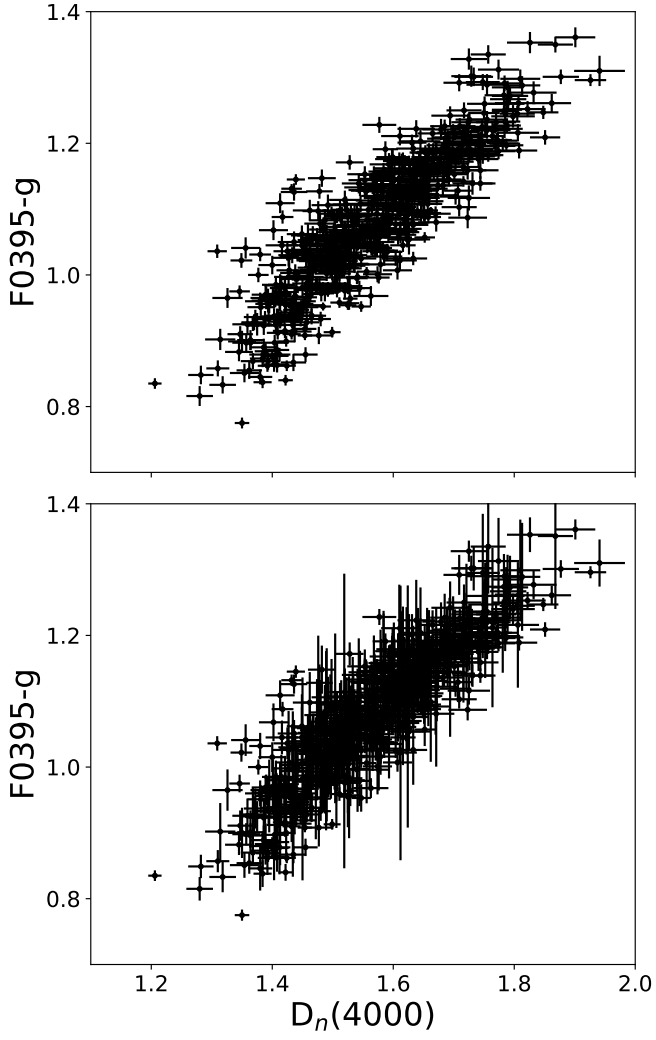


**Fig. 5.** Correlation between the F0395−$g$ colour and the D$_n$(4000) spectral index. *Top panel*: does not take into account internal extinction whereas the *bottom panel* is corrected by dust reddening.

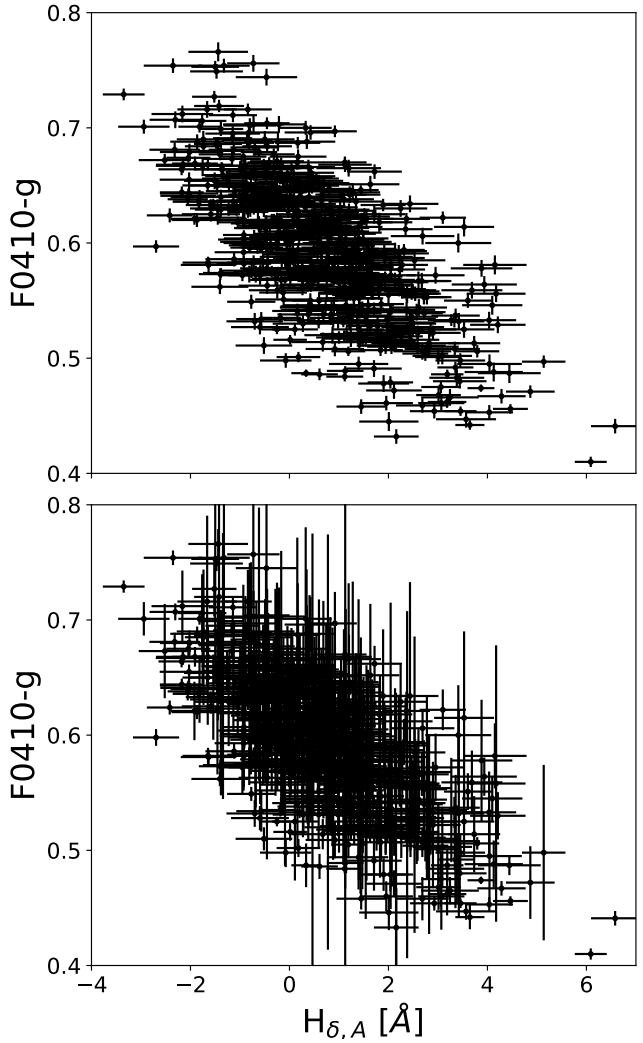


**Fig. 6.** Correlation between the F0410 −$g$ colour and the H$_{\delta,A}$ spectral index, where the F0410 −$g$ colour is corrected (*top panel*) and non-corrected (*bottom panel*) by dust extinction.

morphological classification procedure was based on using the Convolutional Neural Network (CNN) deep learning algorithms. This methodology is able to automatically learn the main characteristics from a training input data. To train the CNN models, Domínguez Sánchez et al. (2018) used the Galaxy Zoo 2 (GZ2; Willett et al. 2013) and Nair & Abraham (2010) catalogues. GZ2 is a citizen science project that used non-professional volunteers to classify thousands of galaxies from SDSS galaxy images. The GZ2 final catalogue contains ∼240 000 galaxies with $m_r < 17$ and $z < 0.25$ from SDSS DR7. The catalogue from Nair & Abraham (2010) comprises ∼14 000 visually classified galaxies from SDSS DR4 within a redshift range of $0.01 < z < 0.1$. The performance of the CNN models were tested using two independent catalogues: the catalogue from Huertas-Company et al. (2011), which classifies ∼670 000 SDSS galaxies by assigning to each galaxy a probability of belonging to one of four morphological classes (E, S0, Sab, and Scd), and the Cheng et al. (2011) catalogue, which contains a combination of visual and automatic morphological classifications of 984 red passive galaxies. We refer the reader to Domínguez Sánchez et al. (2018) for more details about their morphological catalogue.

For each galaxy, Domínguez Sánchez et al. (2018) assign nine different feature probabilities: disc probability ($P_{\rm disc}$), edge-on probability ($P_{\rm edge\text{-}on}$), bar signature probability through GZ2 training sample ($P_{\rm bar\text{-}GZ2}$), bar signature probability through N10 training sample ($P_{\rm bar\text{-}N10}$), merger probability ($P_{\rm merg}$), bulge prominence probability ($P_{\rm bulge}$), cigar-shaped probability ($P_{\rm cigar}$), T-Type classification (connected with Hubble sequence, T-type), and S0 probability ($P_{\rm S0}$). In this work we choose to characterize bar probability $P_{\rm bar\text{-}GZ2}$ rather than $P_{\rm bar\text{-}N10}$. This is because the Galaxy Zoo catalogue provides many more galaxies to calibrate the CNN models and, therefore, we understand that $P_{\rm bar\text{-}GZ2}$ is more reliable than $P_{\rm bar\text{-}N10}$.

### 3.2. Results

From our cross-matched catalogue we pick those with $P_{\rm merg} < 0.5$ and $P_{\rm disc} > 0.5$. With these conditions we aim to select predominantly disc galaxies that do not have a very close companion. We also constrain our sample in terms of stellar mass by choosing those within a mass range of $10^{10.0} < M_\star\,[M_\odot] < 10^{11.0}$. Our sample is complete at $z < 0.075$, as shown in Fig. 9. Martin et al. (2017) discussed that the most massive green valley galaxies ($>10^{11}\,M_\odot$) are probably red sequence galaxies that live at the centre of galaxy groups and clusters; these occasionally capture gas-richer satellite galaxies and consequently

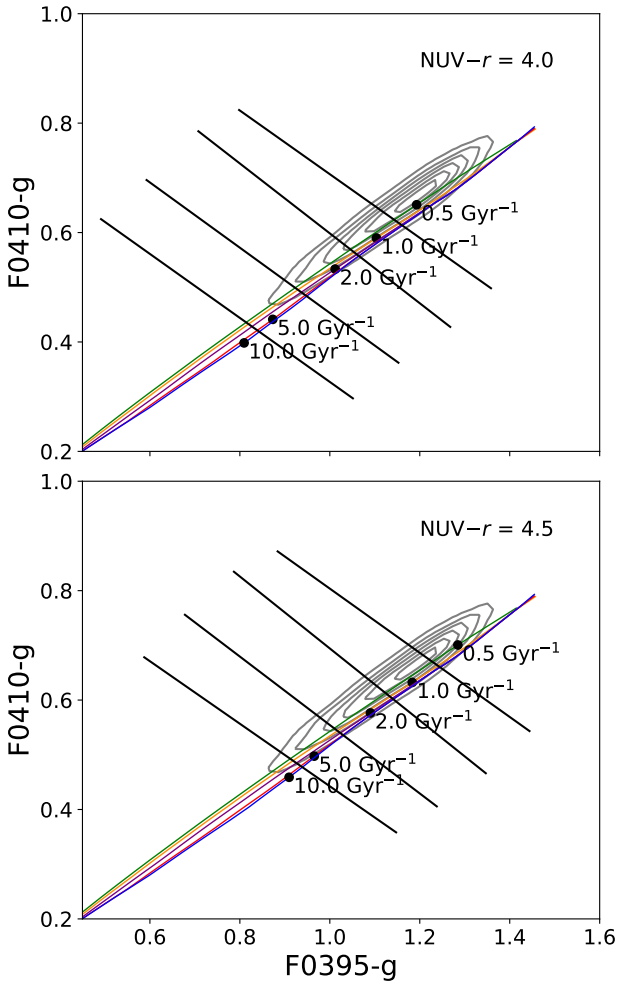


**Fig. 7.** Evolution of the F0410 − $g$ × F0395 − $g$, showing in coloured lines the SFH models presented in Eqs. (5) and (6) with different $\gamma$ values. The black dots and the grey contours are the same as in Fig. 3 for a fixed NUV −$r$ colour.

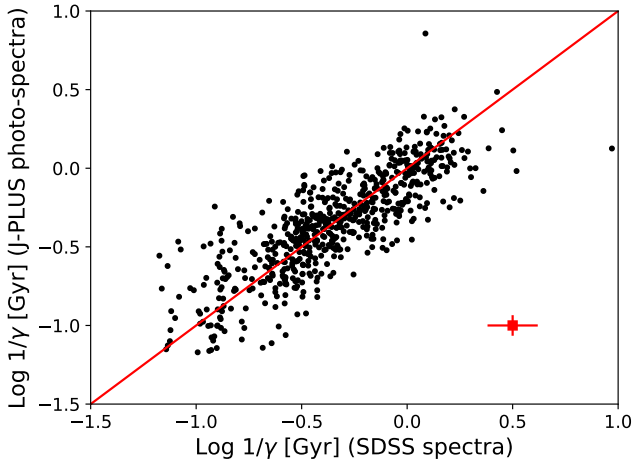


**Fig. 8.** Quenching timescales in green valley galaxies from J-PLUS SEDs versus quenching timescales from spectral indices, for galaxies whose colours are corrected by dust reddening. The red square merely represents the average uncertainties in our estimates. The spearman correlation and the root mean squared error (RMSE) are, respectively, 0.84 and 0.2, indicating a good correlation between the variables.

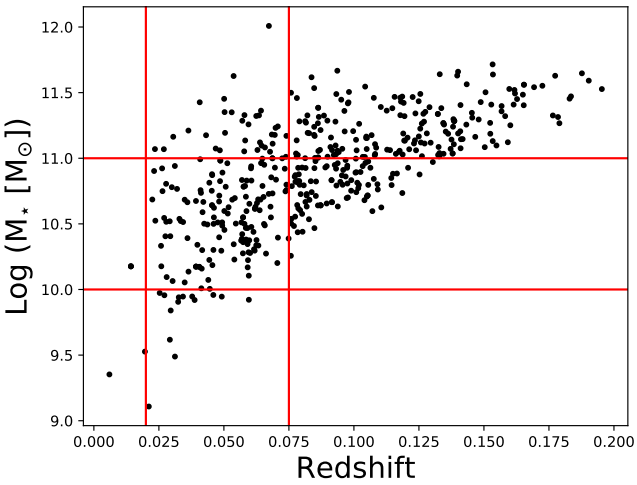


**Fig. 9.** Stellar mass distribution over redshift. The red lines indicate the completeness limits of our sample, with $10 < \log(M_\star\,[M_\odot]) < 11$ and $0.020 < z < 0.075$.

increase temporarily their star formation rate. As we are interested in galaxies that are only quenching their own star formation, we chose to exclude these very massive green valley galaxies. Figure 10 shows the star formation quenching timescales of green valley galaxies as a function of bar probability. For low bar probability the quenching time-scales are spread from low to high values. However, green valley galaxies with higher bar probability ($P_{\rm bar} > 0.3$) tend to have lower quenching timescales. We applied the Kolmogorov−Smirnov test to the distribution of quenching timescales of green valley galaxies with $P_{\rm bar} < 0.1$ (very likely unbarred) and those of $P_{\rm bar} > 0.3$ (very likely barred) to check if these two sub-samples are significantly different. The resulting p-value of 0.006 strongly points against the null hypothesis, meaning they are drawn from the same population, showing that the distribution of quenching timescales of green valley galaxies with low bar probability is indeed statistically different from those of green valley galaxies with high bar probability. We discuss the implications of our findings in the next section.

## 4. Discussions and conclusions

Figure 8 shows that our methodology with J-PLUS filters (F0395, F0410, and gSDSS) can recover quenching timescales in green valley galaxies with good precision in comparison with the methodology from Martin et al. (2007), which uses spectral indices from galaxy spectra. The quenching timescales from our methodology converge with those from Martin et al. (2007) because the F0395, F04010, and $g$SDSS J-PLUS filters cover approximately the same region rest-frame wavelength used to define the $D_n(4000)$ and $H_{\delta,A}$ spectral indices in galaxy spectra. This allows us to use the J-PLUS filters instead of galaxy spectra (Figs. 5 and 6) to drive quenching timescales.

Although both approaches are in agreement, Fig. 8 shows a noticeable dispersion. Nevertheless, our method with J-PLUS filters recovers the quenching timescales with a similar accuracy to that of Martin et al. (2007), in spite of their usage of galaxy spectra. Therefore, Fig. 8 demonstrates the potential of J-PLUS photometry to determine quenching timescales for green valley galaxies in the local Universe. Furthermore, we expect much better constraints with the 56-narrow-band filter system of the upcoming J-PAS survey.

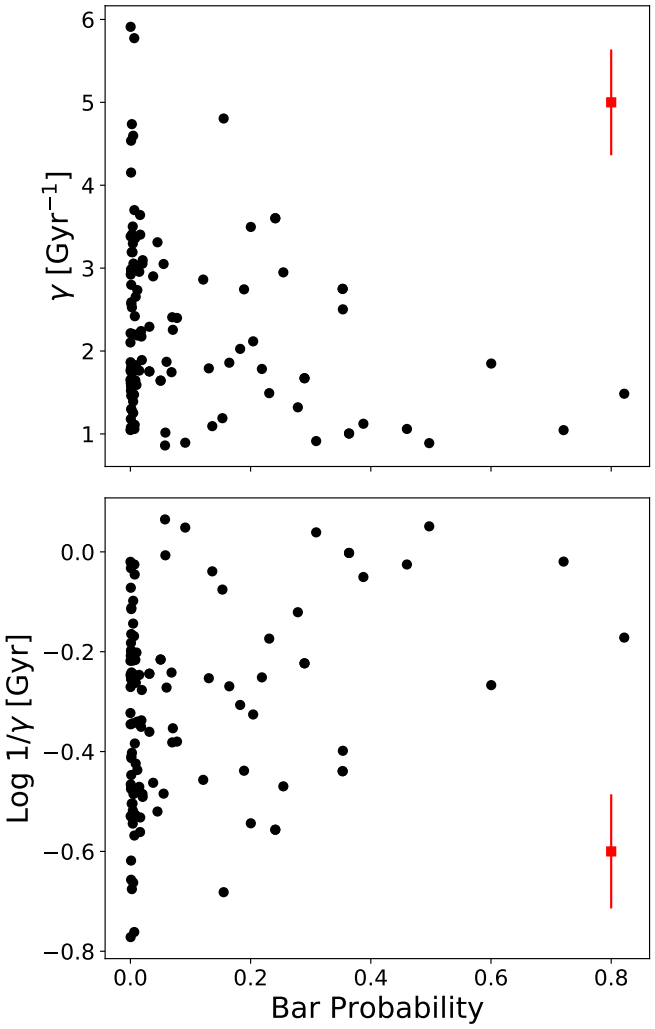


**Fig. 10.** Quenching indices ($\gamma$) and star formation quenching timescales ($1/\gamma$) as functions of bar probability in our sample. The red squares represent the average uncertainty in our sample.

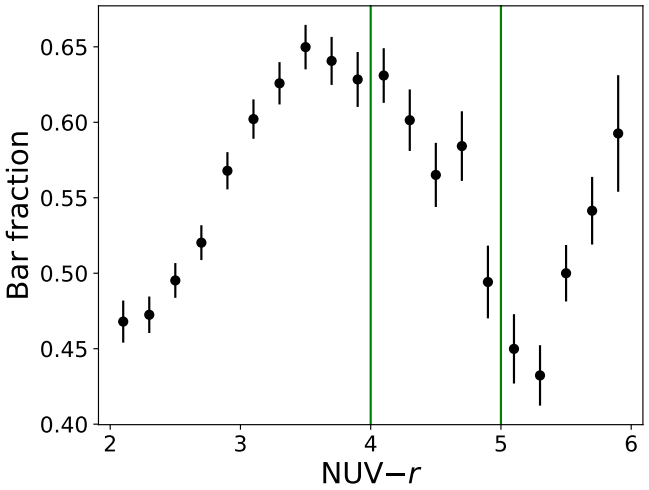


**Fig. 11.** Bar fraction as a function of dust-corrected NUV $-r$ colour. We estimate the error bars as $\sqrt{f(1-f)/N}$ (e.g. Sheth et al. 2008), where $f$ is the bar fraction and $N$ is the total number of galaxies in each colour bin. The green vertical lines delimit the green valley region.

We measured quenching timescales for a set of nearby green valley galaxies and correlated these timescales with the probability of hosting a bar (Fig. 10). The results indicate a tendency for green valley galaxies to have longer quenching timescales for higher bar probability.

In order to better understand the impact of bars in quenching star formation in disc galaxies, we also investigated the bar fraction evolution with NUV $-r$ colour (Fig. 11). We find that the bar fraction behaviour seems to be have an interesting trend with galaxy colour. We note that both within the blue cloud and the red sequence the bar fraction increases towards redder colours by roughly 20%. However, this increase is not continuous across the green valley. Within the green valley we note a significant drop in the bar fraction, resulting in a bar fraction dip at NUV $-r = 6.0$. This general trend we observe in our sample is in agreement with previous works (e.g. Cheung et al. 2013; Kelvin et al. 2018).

### 4.1. Bar formation and evolution

N-body simulations show that bars are naturally formed within 1−2 Gyr or so in dynamically cold discs, although a dark-matter-dominated centre and gas richness may delay this process somewhat (Athanassoula & Sellwood 1986; Athanassoula 2002; Athanassoula et al. 2013; Aumer & Binney 2017). Sheth et al. (2008) found that bar fraction decreases with increasing redshift, consistent with galaxies having a tendency of being more gas rich at higher redshifts (Genzel et al. 2010; Tacconi et al. 2010). As galaxies become more dynamically cold with time, the conditions become more favourable to the formation of a bar. This explains the high value of the local bar fraction in spiral galaxies (~63%; e.g. de Vaucouleurs 1963).

We consider our results from Fig. 11 in the light of this context. With gas richness dropping as we consider redder galaxies in the galaxy CMD, finding a lower bar fraction at the bluer end is reasonable. In fact, recent work by Kruk et al. (2018) shows that unbarred disc galaxies are bluer than barred ones. This is consistent with the increased bar fraction we observe in our sample for galaxies in the blue cloud: galaxies with redder colours within the blue cloud population appear to host bars more frequently. The increase in bar fraction that we observe towards redder red sequence galaxies may also be an extension of this logic. The dip in the bar fraction that appears to characterize the green valley represents an interruption in the otherwise global trend of increasing bar fraction with redder colours. The decrease in the value of the bar fraction within the green valley suggests that processes that lead to the destruction of bars are at work.

Our results displayed in Fig. 11 suggest that bars can form, be destroyed, and form again as galaxies cross the CMD. These same bar-destroying processes must either also be able to quench star formation in galaxies or act in parallel to the processes responsible for quenching star formation. It is interesting to determine the processes responsible for the destruction and the resurgence of bars in disc galaxies.

Over the last couple of decades different studies have pointed to the potential recurrence of the bar phenomenon, where a bar may form, grow in strength, get destroyed (even self-destroy), and ultimately reform in a galaxy disc (Bournaud & Combes 2002; Berentzen et al. 2004; Gadotti & de Souza 2006). Hydrodynamical simulations have shown that the bar-induced increase in mass concentration in the central parts of barred galaxies can lead to bar self-destruction (Roberts et al. 1979; Norman et al. 1996; Sellwood & Moore 1999; Athanassoula et al. 2005). It is worth noting that the amount of central mass concentrations required to effectively accomplish bar destruction are very large

compared to observational constraints (Debattista & Sellwood 2000; Shen & Sellwood 2004; Debattista et al. 2006). Another way of destroying a bar is via tidal interactions with other galaxies (Lee et al. 2012), which may lead to the rapid quenching of star formation (Nogueira-Cavalcante et al. 2018). As galaxies become passive and gas-poor, the discs become susceptible again to the development of a new stellar bar.

It is interesting to consider that the properties of bars in blue cloud barred galaxies have been shown to be different from those in the red sequence: bars in red discs tend to be longer and stronger whereas bars in star-forming discs are usually weaker and show an exponential light profile (Elmegreen & Elmegreen 1985, 1989). This suggests that bars that persist through the galaxy transition from blue to red and through the green valley grow in size and strength. This suggests that, although a portion of the barred galaxies in the blue cloud goes through bar-destroying processes, another portion of the galaxy population has bars that persist through the green valley and continue to grow longer and stronger. The combination of bar survival in some blue cloud galaxies, together with the sequence of bar destruction and renewal in others, would contribute to the increase in bar fraction within the red sequence galaxy population.

We suggest a possible scenario for the transition across the green valley for galaxies with intermediate-mass discs in the local Universe (see schematic representation in Fig. 12). During the blue cloud phase a star-forming galaxy may or may not develop a bar. When quenching processes start to act, barred galaxies may or may not lose their bars. As these galaxies transition through the green valley, the same star formation quenching processes (or other processes acting in parallel) may destroy their bars, driving the bar fraction down (Fig. 11). Galaxies whose bars do not persist through the star formation quenching phase, as well as galaxies that were unbarred within the blue cloud, tend to transit through the green valley (and reach the red sequence) faster than barred green valley galaxies (Fig. 10). Finally, after barred and unbarred galaxies reach the red sequence, barred galaxies tend to retain their bars whereas in unbarred galaxies the conditions become favourable for the formation or resurgence of bars.

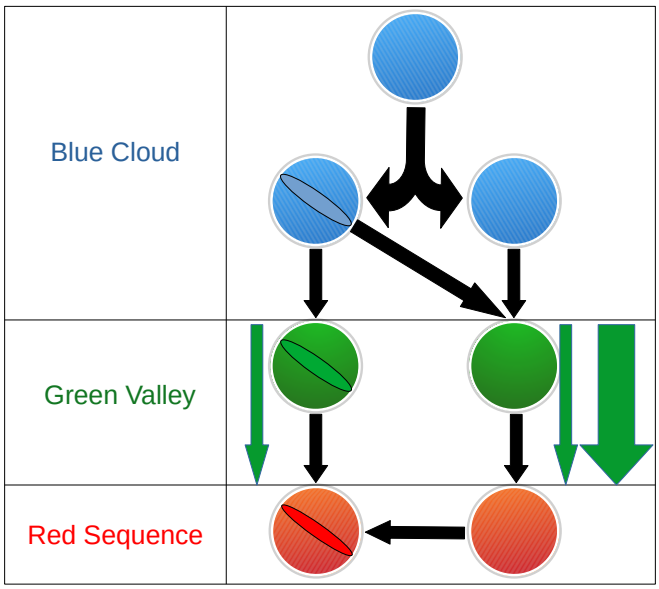


**Fig. 12.** Diagram showing a possible scenario for barred and unbarred discs across the galaxy CMD. Galaxies start their evolution as star-forming blue unbarred galaxies and eventually may or may not develop a bar, depending on internal conditions. When these galaxies enter into the green valley phase, unbarred galaxies remain unbarred whereas many bars in barred galaxies are destroyed (e.g. via interactions). Unbarred disc galaxies can cross slowly or rapidly along the green valley (represented by narrow and wide green arrows, respectively) while barred galaxies only experience slow star formation quenching. When disc galaxies reach the red sequence, barred ones remain barred whereas unbarred ones can develop a new bar.

### 4.2. Bars and star formation quenching

Many previous works have associated bars with quenching star formation. Schawinski et al. (2014) discussed that, amongst disc galaxies, stellar bars can accelerate star formation quenching. Masters et al. (2010) associated quenching with bars in order to explain the high bar fraction amongst passive disc galaxies. Gavazzi et al. (2015) noted that, for nearby disc galaxies, the bar fraction increases with stellar mass. As passive galaxies are more common amongst massive galaxies, these authors suggested that bars may play an important role in quenching star formation. Haywood et al. (2016) claimed that, in the case of our Galaxy, the stellar bar can stabilize the disc, preventing new star formation. Simulations also suggest that bars may efficiently quench star formation, decreasing by a factor of 1 Gyr the star formation rate timescale (Khoperskov et al. 2018).

Although these works suggest that bars induce a faster star formation quenching, our results displayed in Fig. 10 show that green valley disc galaxies with high bar probability tend to quench star formation slowly, which is in agreement with Coelho & Gadotti (2011), who found that the stellar population in bulges of barred galaxies shows an excess of populations younger than ~4 Gyr, when compared to bulges in unbarred galaxies, for the same galaxy masses. Figure 10 also shows that green valley disc galaxies with low bar probability can also quench star formation very slowly and we find that many disc galaxies with low bar probability have quenching timescales greater than those in green valley galaxies with high bar probability. On the other hand, our results suggest that in galaxies with high bar probability the processes which quickly quench star formation are either absent or sustained by the gravitational potential of the host galaxy, which is sufficient to preserve the bar and, simultaneously, the star formation against these processes. Nogueira-Cavalcante et al. (2018) found a similar result for green valley barred galaxies at intermediate redshifts ($0.5 < z < 1.0$), with barred galaxies displaying the longest star formation quenching timescales.

The increase of the bar fraction in the red sequence region (NUV $-r > 5$ in Fig. 11) reflects the greater ease that the red discs have in forming stellar bars. Therefore, bars are probably not associated with accelerated star formation quenching, contrary to simulations, which suggest that bars can increase gas consumption in isolated discs in comparison with unbarred ones (Khoperskov et al. 2018). However, real galaxies are complex structures where several quenching mechanisms (where the majority of them can be bar-destroyers) happen simultaneously. Inevitably, if a disc galaxy remains isolated long enough and keeps the disc dynamically cool, a bar will be formed. Therefore, the barred systems can be interpreted as those where violent physical processes that quench star formation rapidly are absent.

### 4.3. Bar colours impact on the quenching timescales' estimations

In this work we determine the $\gamma$ parameter through the NUV $-r$, F0395 $-g$SDSS and F0410 $-g$SDSS colours. A

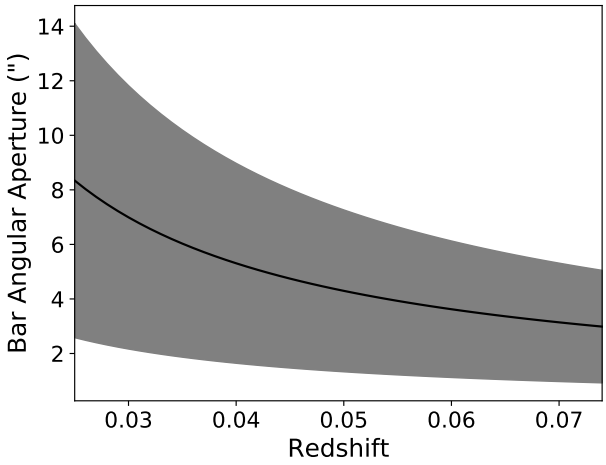


**Fig. 13.** Bar angular aperture of typical barred galaxies as a function of redshift. The solid black line and the grey region represent the average value and the standard deviation of the bar sizes of barred galaxies in the local Universe (Menéndez-Delmestre et al. 2007).

reasonable explanation for the systematic low $\gamma$ values (high quenching timescales) for green valley barred galaxies is that F0395 $-g$SDSS and F0410 $-g$SDSS colours in these galaxies are redder for a specific NUV $-r$ value, in comparison with green valley unbarred galaxies. These reddening F0395 $-g$SDSS and F0410 $-g$SDSS colours could be caused either by dust extinction or by an older stellar population in the bar region in barred galaxies.

To test the dust extinction hypothesis, we analyse the F0395 $-g$SDSS and F0410 $-g$SDSS colours in different angular apertures, in order to compare the central regions (bar region) of unbarred and barred green valley galaxies. The size of bars in a typical disc galaxy in the local Universe is $4.2 \pm 2.9$ kpc (e.g. Menéndez-Delmestre et al. 2007). Figure 13 shows the necessary angular aperture as a function of redshift to cover the bar region of a typical barred galaxy in the local Universe. The aperture photometries available in J-PLUS DR1 are 0.8″, 1.0″, 1.2″, 2.0″, 3.0″, 4.0″, and 6.0″. From Fig. 13 we chose the 3.0″, 4.0″, and 6.0″angular apertures, which cover almost entirely the bar region of typical local barred galaxies over the redshift range of our galaxy sample.

Figures 14 and 15 show the distribution of F0395 $-g$SDSS e F0410 $-g$SDSS colours, respectively, for barred and unbarred green valley galaxies of our sample. From these figures we do not find colour excess for the green valley barred galaxies in the regions delimited by the angular apertures. Therefore, Figs. 14 and 15 suggest that the low $\gamma$ values (Fig. 10) for green valley barred galaxies are due to a more continuous star formation, which simultaneously affects the NUV $-r$, F0395 $-g$SDSS and F0410 $-g$SDSS colours, and not due to dust extinction in the bar region.

To test for a possible bias that could appear from a tentative older stellar population in the bar region, we compare qualitatively the luminosity-weighted age of stellar populations from the bar region and other parts of the galaxy using the Mapping Nearby Galaxies at Apache Point Observatory (MaNGA) data of a sample of face-on barred green valley galaxies. The MaNGA survey (Bundy et al. 2015; Yan et al. 2016) is a SDSS-IV (Blanton et al. 2017) project that aims to obtain spatially resolved spectroscopy for ∼10 000 local galaxies ($z < 0.15$), with a spectral resolution of $R \sim 2000$, from 4000 Å to 8500 Å, using the Baryon Oscillation Spectroscopic Survey spectrograph (BOSS, Smee et al. 2013; Drory et al. 2015) on the Sloan Telescope (Gunn et al. 2006). MaNGA galaxies come from the NASA Sloan Atlas catalogue (NSA; Blanton et al. 2005) that are representative of all the galaxy populations (blue cloud, green valley, and red sequence).

We obtained luminosity-weighted ages from the public MaNGA `FIREFLY` catalogue (Goddard et al. 2017). `FIREFLY` (Fitting IteRativEly For Likelihood analYsis, Wilkinson et al. 2015) is a spectral fitting code that can obtain several stellar population properties from galaxy spectra, such as stellar ages and metallicities. For the spectral fitting `FIREFLY` assumes foreground Milky Way reddening dust maps by Schlegel et al. (1998) and extinction curve by Fitzpatrick (1999), intrinsic reddening by dust in each galaxy by Wilkinson et al. (2015), and stellar population models by Maraston & Strömbäck (2011), with the Medium resolution INT Library of Empirical Spectra stellar library (MILES; Sánchez-Blázquez et al. 2006) and Kroupa initial mass function (Kroupa 2001).

The `FIREFLY` code estimates both luminosity-weighted and mass-weighted stellar ages. The former is sensitive to recent star formation whereas the latter is affected by cumulative galaxy evolution. We decided to use the luminosity-weighted age because recent star formation directly changes galaxy colours and therefore can influence the estimations of quenching timescales.

Figure 16 shows SDSS galaxy images and luminosity-weighted age maps of a sample of face-on barred ($P_{\rm bar} > 0.2$) green valley galaxies identified in the MaNGA `FIREFLY` catalogue. From this figure we do not find any clear indication that the bar region is systematically older (redder) than the other parts of the galaxy. Therefore the quenching timescales from Fig. 10 for barred green valley galaxies very likely reflect the overall galaxy evolution.

### 4.4. Photo-$z$ impact on the quenching timescales' estimations

Another legacy of J-PLUS will be marked by the photometric redshift determination of galaxies. We explore the impact of photo-$z$ uncertainties when computing quenching timescales with J-PLUS data. The photometric redshifts are calculated using the BPZ code (Benítez 2000). Figure 17 shows the correlation between the quenching timescales obtained with spectroscopic redshifts with those obtained with photo-$z$. We find that for the majority of green valley galaxies we can recover approximately the same timescales, demonstrating that the photo-$z$ uncertainties' impact is very small in estimations of quenching timescales.

## 5. Summary

The scarcity of galaxies between the blue and red peaks on galaxy CMD (green valley) and the growth of the red sequence (at least from $z \sim 2$) indicate that galaxy transition across the green valley is rapid and continuous. The identification of the physical processes that are able to transform galaxies from star forming to passive systems still remains a challenge to galaxy formation and evolution models. Stellar bars are one of the possible physical processes that could accelerate gas depletion and consequently quench star formation faster. In this work we adapted the method of Martin et al. (2007) – which is able to estimate star formation quenching timescales in green valley galaxies based on spectroscopic data – to the photometric data from J-PLUS and GALEX surveys. Through this method, we

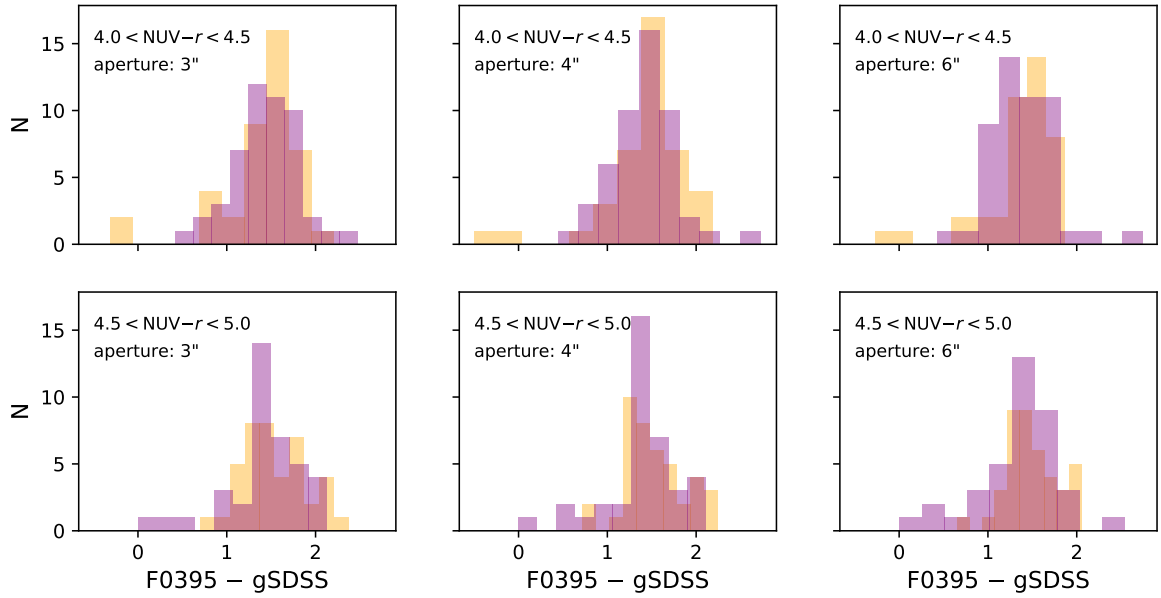


**Fig. 14.** Distributions of the F0395 $-g$SDSS colour for barred (purple) and unbarred (orange) green valley galaxies for different angular apertures and NUV $-r$ colour ranges.

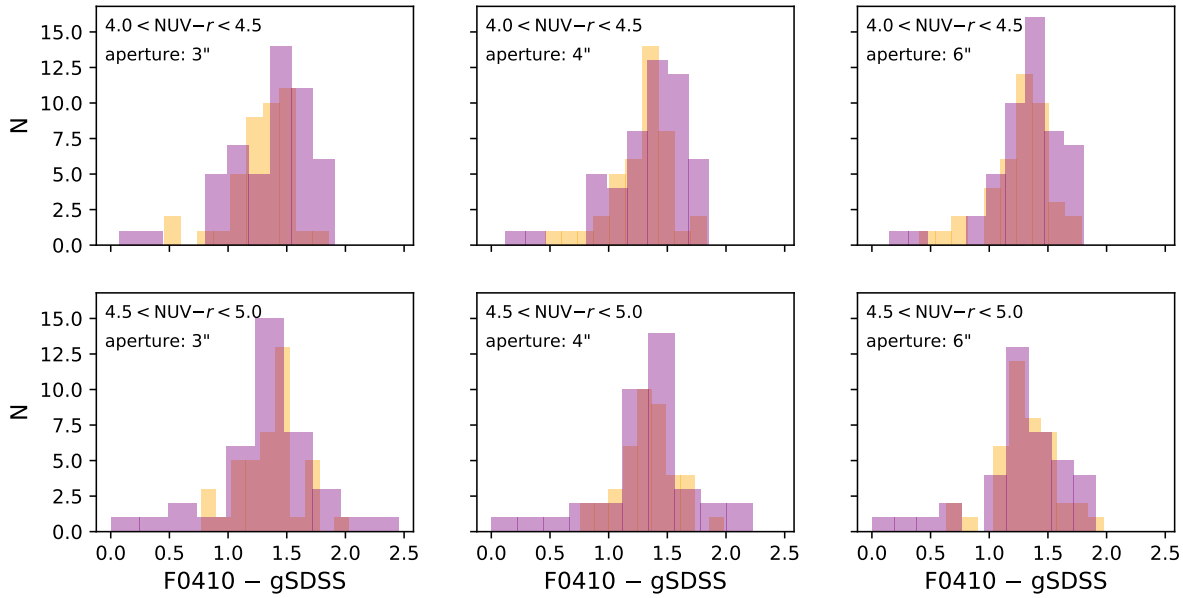


**Fig. 15.** Same in the Fig. 14 for the F0410 $-g$SDSS colours.

measured quenching timescales of nearby green valley galaxies ($0.022 < z < 0.075$) and we correlated these timescales with the probability of these galaxies hosting a bar (bar probability).

Our main results are:

1. Our method using photometric data is able to estimate quenching timescales at the same precision level as that of Martin et al. (2007), which assesses quenching timescales from galaxy spectra.
2. We find a strong correlation between quenching timescales and bar probability of green valley disc galaxies. Quenching timescales amongst green valley galaxies with low bar probability have a large scatter whereas for high bar probability green valley disc galaxies tend to have long quenching timescales. These results suggest that violent quenching processes, which are able to simultaneously destroy the bars and quench star formation quickly, are absent, or the gravitational potential of the host galaxy is strong enough to maintain both the stellar bar and a more stable star formation.
3. The apparent bar bimodality with NUV $-r$ colour indicates potential different bar phases. During the blue cloud phase, bars are naturally formed, which is reflected by the increase of bar fraction with colour, until NUV $-r \sim 3.5$. After this peak, bar fraction quickly decreases, reaching a minimum at the beginning of red sequence phase (NUV $-r \sim 5.2$). This suggests that the same quenching processes that move galaxies across the green valley can also destroy the bars or bar-destroying processes happen simultaneously with quenching processes. Red sequence discs can recover their bars, as indicated by the increase of bar fraction in NUV $-r > 5.2$.

Our analysis of quenching timescales as a function of bar probability in nearby green valley galaxies and bar fraction as a function of NUV $-r$ colour suggests an evolutionary scenario

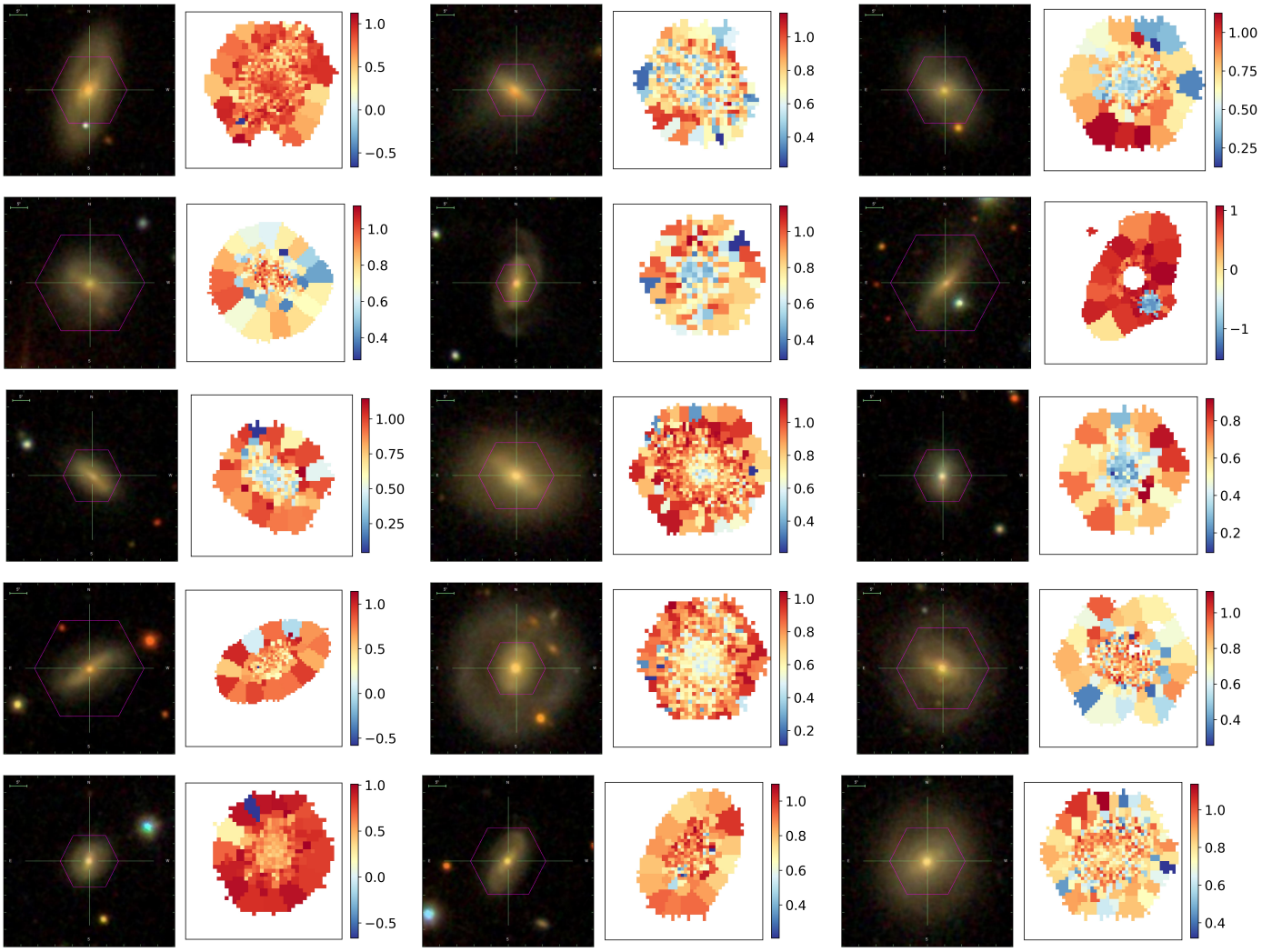

**Fig. 16.** Sloan Digital Sky Survey galaxy images and luminosity-weighted stellar ages of a sample of face-on barred green valley galaxies. The purple hexagon indicates the MaNGA field of view and the luminosity-weighted ages are expressed in $\log_{10}$(age[Gyr]).

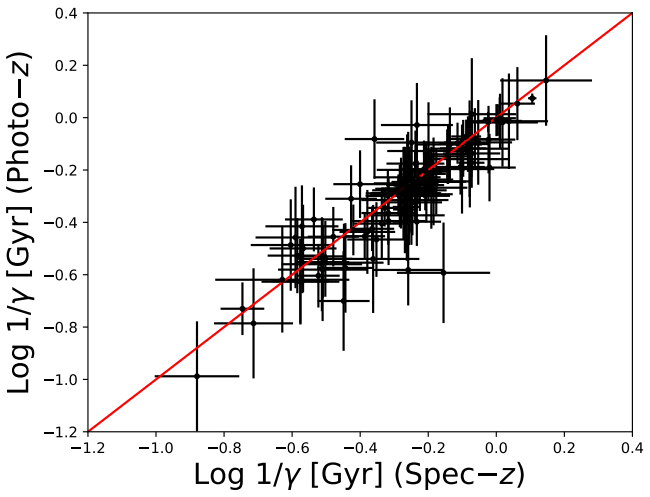


**Fig. 17.** Comparison of quenching timescales based on photometric and spectroscopic redshifts.The spearman correlation and RMSE are, respectively, 0.89 and 0.09.

(Fig. 12) where massive disc galaxies ($10^{10} < M\,[M_\odot] < 10^{11.5}$) quench their star formation in slow mode, whereas unbarred galaxies can quench their star formation both in slow and fast modes. Future surveys, such as the recently started J-PAS, can perhaps address this scenario in galaxy-dense environments.

*Acknowledgements.* We thank the anonymous referee for contributing to improving our paper. JPNC was supported by a Institutional Capacity Programme grant from CNPq – the Brazilian National Council for Scientific and Technological Development – within the Ministry of Education of Brazil and Ministry of Science, Technology, Innovations, and Communication. RD acknowledges support from the CNPq through BP grant 312307/2015-2, and the Financiadora de Estudos e Projetos – FINEP grants REF. 1217/13 - 01.13.0279.00 and REF 0859/10 – 01.10.0663.00 for hardware support for the J-PLUS project through the National Observatory of Brazil and CBPF. PC acknowledges support from FAPESP 2018/05392-8, CNPq 305066/2015-3, and USP/Cofecub 18.1.214.1.8/40449YB. MLLD acknowledges *Coordenação de Aperfeiçoamento de Pessoal de Nível Superior* – Brasil (CAPES) – Finance Code 001, *Conselho Nacional de Desenvolvimento Científico e Tecnológico* (CNPq). KMD thanks the support of the CNPq. JHJ thanks the Brazilian institution CNPq for financial support through a postdoctoral fellowship (project 150237/2017-0) and the Chilean institution CONICYT, Programa de Astronomía, Fondo ALMA-CONICYT 2017, Código de proyecto 31170038. ET was supported by ETAg grants IUT40-2, IUT26-2, and by the EU through the ERDF CoE grant TK133 and MOBTP86. This research made use of the "*k*-corrections calculator" service available at `http://kcor.sai.msu.ru/`. `Python` wrapper of the `C` library by Blanton & Roweis (2007), with `Python` wrapper on github (`https://pypi.python.org/pypi/kcorrect_python/2017.07.05`). Based on observations made with the JAST/T80 telescope at the Observatorio Astrofísico de Javalambre (OAJ) in Teruel, owned, managed, and operated by the Centro

de Estudios de Física del Cosmos de Aragón. We acknowledge the OAJ Data Processing and Archiving Unit (UPAD) for reducing and calibrating the OAJ data used in this work. Funding for the J-PLUS Project has been provided by the Governments of Spain and Aragón through the Fondo de Inversiones de Teruel; the Aragón Government through the Reseach Groups E96, E103, and E16_17R; the Spanish Ministry of Science, Innovation and Universities (MCIU/AEI/FEDER, UE) with grants PGC2018-097585-B-C21 and PGC2018-097585-B-C22, the Spanish Ministry of Economy and Competitiveness (MINECO) under AYA2015-66211-C2-1-P, AYA2015-66211-C2-2, AYA2012-30789, and ICTS-2009-14; and European FEDER funding (FCDD10-4E-867, FCDD13-4E-2685). Funding for the SDSS and SDSS-II has been provided by the Alfred P. Sloan Foundation, the Participating Institutions, the National Science Foundation, the U.S. Department of Energy, the National Aeronautics and Space Administration, the Japanese Monbukagakusho, the Max Planck Society, and the Higher Education Funding Council for England. The SDSS Web Site is www.sdss.org. The SDSS is managed by the Astrophysical Research Consortium for the Participating Institutions. The Participating Institutions are the American Museum of Natural History, Astrophysical Institute Potsdam, University of Basel, University of Cambridge, Case Western Reserve University, University of Chicago, Drexel University, Fermilab, the Institute for Advanced Study, the Japan Participation Group, Johns Hopkins University, the Joint Institute for Nuclear Astrophysics, the Kavli Institute for Particle Astrophysics and Cosmology, the Korean Scientist Group, the Chinese Academy of Sciences (LAMOST), Los Alamos National Laboratory, the Max-Planck-Institute for Astronomy (MPIA), the Max-Planck-Institute for Astrophysics (MPA), New Mexico State University, the Ohio State University, University of Pittsburgh, University of Portsmouth, Princeton University, the United States Naval Observatory, and the University of Washington. This research is based on observations made with the Galaxy Evolution Explorer, obtained from the MAST data archive at the Space Telescope Science Institute, which is operated by the Association of Universities for Research in Astronomy, Inc., under NASA contract NAS 5-26555.

## References

Abadi, M. G., Moore, B., & Bower, R. G. 1999, MNRAS, 308, 947
Aguerri, J. A. L., Méndez-Abreu, J., & Corsini, E. M. 2009, A&A, 495, 491
Alam, S., Albareti, F. D., Allende Prieto, C., et al. 2015, ApJS, 219, 12
Alongi, M., Bertelli, G., Bressan, A., et al. 1993, A&AS, 97, 851
Athanassoula, E. 2002, ApJ, 569, L83
Athanassoula, E. 2003, MNRAS, 341, 1179
Athanassoula, E., & Sellwood, J. A. 1986, MNRAS, 221, 213
Athanassoula, E., Lambert, J. C., & Dehnen, W. 2005, MNRAS, 363, 496
Athanassoula, E., Machado, R. E. G., & Rodionov, S. A. 2013, MNRAS, 429, 1949
Aumer, M., & Binney, J. 2017, MNRAS, 470, 2113
Baldry, I. K., Glazebrook, K., Brinkmann, J., et al. 2004, ApJ, 600, 681
Balogh, M. L., Morris, S. L., Yee, H. K. C., Carlberg, R. G., & Ellingson, E. 1999, ApJ, 527, 54
Balogh, M. L., Baldry, I. K., Nichol, R., et al. 2004, ApJ, 615, L101
Bell, E. F., Wolf, C., Meisenheimer, K., et al. 2004, ApJ, 608, 752
Benítez, N. 2000, ApJ, 536, 571
Benitez, N., Dupke, R., Moles, M., et al. 2014, ArXiv e-prints [arXiv:1403.5237]
Berentzen, I., Athanassoula, E., Heller, C. H., & Fricke, K. J. 2004, MNRAS, 347, 220
Blanton, M. R., & Roweis, S. 2007, AJ, 133, 734
Blanton, M. R., Schlegel, D. J., Strauss, M. A., et al. 2005, AJ, 129, 2562
Blanton, M. R., Bershady, M. A., Abolfathi, B., et al. 2017, AJ, 154, 28
Bongiorno, A., Schulze, A., Merloni, A., et al. 2016, A&A, 588, A78
Boselli, A., Boissier, S., Cortese, L., et al. 2006, ApJ, 651, 811
Bournaud, F., & Combes, F. 2002, A&A, 392, 83
Brammer, G. B., Whitaker, K. E., van Dokkum, P. G., et al. 2009, ApJ, 706, L173
Bremer, M. N., Phillipps, S., Kelvin, L. S., et al. 2018, MNRAS, 476, 12
Bressan, A., Fagotto, F., Bertelli, G., & Chiosi, C. 1993, A&AS, 100, 647
Brinchmann, J., Charlot, S., White, S. D. M., et al. 2004, MNRAS, 351, 1151
Brown, M. J. I., Dey, A., Jannuzi, B. T., et al. 2007, ApJ, 654, 858
Bruzual, G., & Charlot, S. 2003, MNRAS, 344, 1000
Bruzual, G. 1983, ApJ, 273, 105
Bundy, K., Bershady, M. A., Law, D. R., et al. 2015, ApJ, 798, 7
Calzetti, D., Kinney, A. L., & Storchi-Bergmann, T. 1994, ApJ, 429, 582
Calzetti, D., Armus, L., Bohlin, R. C., et al. 2000, ApJ, 533, 682
Capak, P., Aussel, H., Ajiki, M., et al. 2007, ApJS, 172, 99
Cattaneo, A., Faber, S. M., Binney, J., et al. 2009, Nature, 460, 213
Cenarro, A. J., Moles, M., Cristóbal-Hornillos, D., et al. 2019, A&A, 622, A176
Chabrier, G. 2003, ApJ, 586, L133
Cheng, J. Y., Faber, S. M., Simard, L., et al. 2011, MNRAS, 412, 727
Cheung, E., Athanassoula, E., Masters, K. L., et al. 2013, ApJ, 779, 162
Chilingarian, I. V., & Zolotukhin, I. Y. 2012, MNRAS, 419, 1727
Chilingarian, I. V., Melchior, A.-L., & Zolotukhin, I. Y. 2010, MNRAS, 405, 1409
Ciotti, L., & Ostriker, J. P. 2007, ApJ, 665, 1038
Coelho, P., & Gadotti, D. A. 2011, ApJ, 743, L13
Conselice, C. J. 2006, ApJ, 638, 686
Darvish, B., Martin, C., Gonçalves, T. S., et al. 2018, ApJ, 853, 155
Darvish, B., Mobasher, B., Sobral, D., et al. 2016, ApJ, 825, 113
de Vaucouleurs, G. 1963, ApJS, 8, 31
Debattista, V. P., Mayer, L., Carollo, C. M., et al. 2006, ApJ, 645, 209
Debattista, V. P., & Sellwood, J. A. 2000, ApJ, 543, 704
Dekel, A., & Burkert, A. 2014, MNRAS, 438, 1870
Di Matteo, T., Springel, V., & Hernquist, L. 2005, Nature, 433, 604
Díaz-García, L. A., Cenarro, A. J., López-Sanjuan, C., et al. 2018, A&A, submitted [arXiv:1711.10590]
Domínguez Sánchez, H., Huertas-Company, M., Bernardi, M., Tuccillo, D., & Fischer, J. L. 2018, MNRAS, 476, 3661
Drory, N., MacDonald, N., Bershady, M. A., et al. 2015, AJ, 149, 77
Dubois, Y., Gavazzi, R., Peirani, S., & Silk, J. 2013, MNRAS, 433, 3297
Elmegreen, B. G., & Elmegreen, D. M. 1985, ApJ, 288, 438
Elmegreen, B. G., & Elmegreen, D. M. 1989, ApJ, 342, 677
Evans, F. A., Parker, L. C., & Roberts, I. D. 2018, MNRAS, 476, 5284
Faber, S. M., Willmer, C. N. A., Wolf, C., et al. 2007, ApJ, 665, 265
Fagotto, F., Bressan, A., Bertelli, G., & Chiosi, C. 1994a, A&AS, 105, 29
Fagotto, F., Bressan, A., Bertelli, G., & Chiosi, C. 1994b, A&AS, 104, 365
Fitzpatrick, E. L. 1999, PASP, 111, 63
Gadotti, D. A., & de Souza, R. E. 2006, ApJS, 163, 270
Gavazzi, G., Consolandi, G., Dotti, M., et al. 2015, A&A, 580, A116
Genzel, R., Tacconi, L. J., Gracia-Carpio, J., et al. 2010, MNRAS, 407, 2091
Gilbank, D. G., Balogh, M. L., Glazebrook, K., et al. 2010, MNRAS, 405, 2419
Goddard, D., Thomas, D., Maraston, C., et al. 2017, MNRAS, 466, 4731
Gonçalves, T. S., Martin, D. C., Menéndez-Delmestre, K., Wyder, T. K., & Koekemoer, A. 2012, ApJ, 759, 67
Gunn, J. E., & Gott, III., J. R. 1972, ApJ, 176, 1
Gunn, J. E., Siegmund, W. A., Mannery, E. J., et al. 2006, AJ, 131, 2332
Hatfield, P. W., & Jarvis, M. J. 2017, MNRAS, 472, 3570
Hausman, M. A., & Ostriker, J. P. 1978, ApJ, 224, 320
Haywood, M., Lehnert, M. D., Di Matteo, P., et al. 2016, A&A, 589, A66
Ho, L. C., Filippenko, A. V., & Sargent, W. L. W. 1997, ApJ, 487, 591
Huertas-Company, M., Aguerri, J. A. L., Bernardi, M., Mei, S., & Sánchez Almeida, J. 2011, A&A, 525, A157
Ilbert, O., McCracken, H. J., Le Fèvre, O., et al. 2013, A&A, 556, A55
Kauffmann, G., Heckman, T. M., White, S. D. M., et al. 2003, MNRAS, 341, 33
Kelvin, L. S., Bremer, M. N., Phillipps, S., et al. 2018, MNRAS, 477, 4116
Khoperskov, S., Haywood, M., Di Matteo, P., Lehnert, M. D., & Combes, F. 2018, A&A, 609, A60
Kocevski, D. D., Barro, G., Faber, S. M., et al. 2017, ApJ, 846, 112
Kormendy, J., & Kennicutt, Jr., R. C. 2004, ARA&A, 42, 603
Kroupa, P. 2001, MNRAS, 322, 231
Kruk, S. J., Lintott, C. J., Bamford, S. P., et al. 2018, MNRAS, 473, 4731
Lagos, C. D. P., Lacey, C. G., & Baugh, C. M. 2013, MNRAS, 436, 1787
Lee, G.-H., Park, C., Lee, M. G., & Choi, Y.-Y. 2012, ApJ, 745, 125
Lilly, S. J., Le Fèvre, O., Renzini, A., et al. 2007, ApJS, 172, 70
Lim, P. L., Diaz, R. I., & Laidler, V. 2015, PySynphot User's Guide
Machado, R. E. G., & Athanassoula, E. 2010, MNRAS, 406, 2386
Madau, P., & Dickinson, M. 2014, ARA&A, 52, 415
Maltby, D. T., Almaini, O., Wild, V., et al. 2018, MNRAS, 480, 381
Maraston, C., & Strömbäck, G. 2011, MNRAS, 418, 2785
Martin, D. C., Fanson, J., Schiminovich, D., et al. 2005, ApJ, 619, L1
Martin, D. C., Wyder, T. K., Schiminovich, D., et al. 2007, ApJS, 173, 342
Martin, D. C., Gonçalves, T. S., Darvish, B., Seibert, M., & Schiminovich, D. 2017, ApJ, 842, 20
Masters, K. L., Mosleh, M., Romer, A. K., et al. 2010, MNRAS, 405, 783
Masters, K. L., Nichol, R. C., Hoyle, B., et al. 2011, MNRAS, 411, 2026
McGee, S. L., Balogh, M. L., Wilman, D. J., et al. 2011, MNRAS, 413, 996
Menci, N., Fontana, A., Giallongo, E., & Salimbeni, S. 2005, ApJ, 632, 49
Mendez, A. J., Coil, A. L., Lotz, J., et al. 2011, ApJ, 736, 110
Méndez-Abreu, J., Aguerri, J. A. L., Corsini, E. M., & Simonneau, E. 2008, A&A, 478, 353
Menéndez-Delmestre, K., Sheth, K., Schinnerer, E., Jarrett, T. H., & Scoville, N. Z. 2007, ApJ, 657, 790
Moore, B., Lake, G., & Katz, N. 1998, ApJ, 495, 139
Moran, S. M., Ellis, R. S., Treu, T., et al. 2007, ApJ, 671, 1503
Muzzin, A., Marchesini, D., Stefanon, M., et al. 2013, ApJ, 777, 18
Nair, P. B., & Abraham, R. G. 2010, ApJS, 186, 427
Noeske, K. G., Weiner, B. J., Faber, S. M., et al. 2007, ApJ, 660, L43

Nogueira-Cavalcante, J. P., Gonçalves, T. S., Menéndez-Delmestre, K., & Sheth, K. 2018, MNRAS, 473, 1346
Nogueira-Cavalcante, J. P., Gonçalves, T. S., Menéndez-Delmestre, K., de la Rosa, I. G., & Charbonnier, A. 2019, MNRAS, 484, 3022
Norman, C. A., Sellwood, J. A., & Hasan, H. 1996, ApJ, 462, 114
Oh, S., Oh, K., & Yi, S. K. 2012, ApJS, 198, 4
Pan, Z., Kong, X., & Fan, L. 2013, ApJ, 776, 14
Pan, Z., Li, J., Lin, W., Wang, J., & Kong, X. 2014, ApJ, 792, L4
Peng, Y., Maiolino, R., & Cochrane, R. 2015, Nature, 521, 192
Peng, Y.-J., Lilly, S. J., Kovač, K., et al. 2010, ApJ, 721, 193
Renzini, A., & Peng, Y.-J. 2015, ApJ, 801, L29
Roberts, Jr., W. W., Huntley, J. M., & van Albada, G. D. 1979, ApJ, 233, 67
Rowlands, K., Wild, V., Bourne, N., et al. 2018, MNRAS, 473, 1168
Salim, S. 2014, Astron. J., 189, 1
Salim, S., Rich, R. M., Charlot, S., et al. 2007, ApJS, 173, 267
Sánchez-Blázquez, P., Peletier, R. F., Jiménez-Vicente, J., et al. 2006, MNRAS, 371, 703
Schawinski, K., Lintott, C. J., Thomas, D., et al. 2009, ApJ, 690, 1672
Schawinski, K., Urry, C. M., Simmons, B. D., et al. 2014, MNRAS, 440, 889
Schlegel, D. J., Finkbeiner, D. P., & Davis, M. 1998, ApJ, 500, 525
Seaton, M. J. 1979, MNRAS, 187, 73P
Sellwood, J. A. 1981, A&A, 99, 362
Sellwood, J. A., & Moore, E. M. 1999, ApJ, 510, 125
Shen, J., & Sellwood, J. A. 2004, ApJ, 604, 614
Shen, S., Mo, H. J., White, S. D. M., et al. 2003, MNRAS, 343, 978
Sheth, K., Vogel, S. N., Regan, M. W., Thornley, M. D., & Teuben, P. J. 2005, ApJ, 632, 217
Sheth, K., Elmegreen, D. M., Elmegreen, B. G., et al. 2008, ApJ, 675, 1141
Shlosman, I., Frank, J., & Begelman, M. C. 1989, Nature, 338, 45
Smee, S. A., Gunn, J. E., Uomoto, A., et al. 2013, AJ, 146, 32
Smethurst, R. J., Lintott, C. J., Simmons, B. D., et al. 2015, MNRAS, 450, 435
Smethurst, R. J., Lintott, C. J., Simmons, B. D., et al. 2016, MNRAS, 463, 2986
Smethurst, R. J., Lintott, C. J., Bamford, S. P., et al. 2017, MNRAS, 469, 3670
Sobral, D., Best, P. N., Smail, I., et al. 2014, MNRAS, 437, 3516
Speagle, J. S., Steinhardt, C. L., Capak, P. L., & Silverman, J. D. 2014, ApJS, 214, 15
Springel, V., Di Matteo, T., & Hernquist, L. 2005a, ApJ, 620, L79
Springel, V., Di Matteo, T., & Hernquist, L. 2005b, ApJ, 620, L79
Straatman, C. M. S., van der Wel, A., Bezanson, R., et al. 2018, ApJS, 239, 27
Strateva, I., Ivezić, Ž., Knapp, G. R., et al. 2001, AJ, 122, 1861
STScI development Team 2013, Astrophysics Source Code Library [record ascl:1303.023]
Tacconi, L. J., Genzel, R., Neri, R., et al. 2010, Nature, 463, 781
Taylor, E. N., Franx, M., van Dokkum, P. G., et al. 2009, ApJ, 694, 1171
Toomre, A. 1977, in Evolution of Galaxies and Stellar Populations, eds. B. M. Tinsley, R. B. G. Larson, & D. Campbell, 401
Trayford, J. W., Theuns, T., Bower, R. G., et al. 2016, MNRAS, 460, 3925
van de Voort, F., Bahé, Y. M., Bower, R. G., et al. 2017, MNRAS, 466, 3460
van den Bosch, F. C., Aquino, D., Yang, X., et al. 2008, MNRAS, 387, 79
van der Wel, A., Noeske, K., Bezanson, R., et al. 2016, ApJS, 223, 29
Wang, J., Kauffmann, G., Overzier, R., et al. 2012, MNRAS, 423, 3486
Wetzel, A. R., Tinker, J. L., Conroy, C., & van den Bosch, F. C. 2013, MNRAS, 432, 336
Whitaker, K. E., Kriek, M., van Dokkum, P. G., et al. 2012, ApJ, 745, 179
White, S. D. M. 1976, MNRAS, 174, 19
Wilkinson, D. M., Maraston, C., Thomas, D., et al. 2015, MNRAS, 449, 328
Willett, K. W., Lintott, C. J., Bamford, S. P., et al. 2013, MNRAS, 435, 2835
Willmer, C. N. A., Faber, S. M., Koo, D. C., et al. 2006, ApJ, 647, 853
Worthey, G., & Ottaviani, D. L. 1997, ApJS, 111, 377
Wyder, T. K., Martin, D. C., Schiminovich, D., et al. 2007, ApJS, 173, 293
Yan, R., Bundy, K., Law, D. R., et al. 2016, AJ, 152, 197
York, D. G., Adelman, J., Anderson, Jr., J. E., et al. 2000, AJ, 120, 1579
Zolotov, A., Dekel, A., Mandelker, N., et al. 2015, MNRAS, 450, 2327

[1] Observatório Nacional, Rua General José Cristino 77, Rio de Janeiro, RJ 20921-400, Brazil
e-mail: jpncavalcante@gmail.com
[2] University of Michigan, Ann Arbor, MI 48109-1090, USA
[3] Instituto de Astronomia, Geofísica e Ciências Atmosféricas, Universidade de São Paulo, São Paulo, SP 05508-090, Brazil
[4] Departamento de Física Teórica, Universidad Autónoma de Madrid, 28049 Madrid, Spain
[5] Observatório do Valongo, Universidade Federal do Rio de Janeiro, Ladeira Pedro Antônio 43, Rio de Janeiro, RJ 20080-090, Brazil
[6] Departamento de Física, Universidade Federal de Sergipe, São Cristóvão, SE, Brazil
[7] Lancaster University, Lancaster LA1 4YB, UK
[8] Departamento de Astronomia, Universidade Federal do Rio Grande do Sul, Av. Bento Gonçalves 9500, Porto Alegre, RS 91501-970, Brazil
[9] Departamento de Ciencias Fisicas, Universidad Andres Bello, 700 Fernandez Concha, Las Condes, Santiago, Chile
[10] Tartu Observatory, University of Tartu,Observatooriumi 1, 61602 Tõravere, Estonia
[11] Departamento de Física Teórica, Universidad Autónoma de Madrid, Madrid 28049, Spain
[12] Centro de Estudios de Física del Cosmos de Aragón (CEFCA), Unidad Asociada al CSIC, Plaza San Juan 1, 44001 Teruel, Spain
[13] European Space Astronomy Centre (ESAC)/ESA, Madrid, Spain
[14] PITT PACC, Department of Physics and Astronomy, University of Pittsburgh, Pittsburgh, PA 15260, USA
[15] DIPC, Paseo Manuel de Lardizabal 4, 20018 Donostia-san Sebastián, Spain
[16] Center for Space Science and Technology, University of Maryland, Baltimore County, 1000 Hilltop Circle, Baltimore, MD 21250, USA